Diffusion of hard sphere fluids in disordered media: A molecular dynamics simulation study

Rakwoo Chang, Kamakshi Jagannathan, and Arun Yethiraj
Theoretical Chemistry Institute and Department of Chemistry, University of Wisconsin, Madison, Wisconsin 53706, USA
(Received 6 November 2004; published 6 May 2004)

Molecular dynamic simulations are reported for the static and dynamic properties of hard sphere fluids in matrices (or media) composed of quenched hard spheres. The effect of fluid and matrix density, matrix structure, and fluid to matrix sphere size ratio on the static and dynamic properties is studied using discontinuous molecular dynamics. The matrix density has a stronger effect on the self-diffusion coefficient than the fluid density, especially at high matrix densities where the geometric constraints due to the quenched spheres are significant. When the ratio of the size of the fluid spheres to that of the matrix spheres is equal to or greater than one, the diffusion increases as the fluid density is increased, at constant total volume fraction. This trend is however reversed if the ratio is smaller than one. Different methods of generating the matrix have a very strong effect on the dynamic properties even though the static correlations are similar. An analysis of the single-chain structure factor of the particle trajectories shows a change in the particle diffusive behavior at different time scales, suggestive of a hopping mechanism, although normal diffusion is recovered at long times. At high matrix densities, there is considerable heterogeneity in the diffusion of the fluid particles. The simulations demonstrate that the correlations in the matrix play a significant role on the diffusion of fluid spheres. For example, the diffusion constant in matrices constructed by different methods can be an order of magnitude different even though the pair correlation functions are almost identical.

DOI: 10.1103/PhysRevE.69.051101 PACS number(s): 46.65.+g

I. INTRODUCTION

The behavior of fluids in complex environments is of significance in numerous situations ranging from analytical separations and industry to the fundamentals of transport in living cells and heterogeneous materials. For example, in analytical separations one is interested in separating species that are very similar in their physical properties by taking advantage of small differences in their adsorption and transport through a matrix, such as a gel or polymer solution. A molecular understanding of the effect of the matrix structure and interaction of the matrix with solutes on the adsorption and transport can go a long way in establishing the relative importance of structural and interaction effects on the adsorption and dynamics of solutes. Despite the importance of these systems, there has been very little theoretical or computational research on the dynamics of fluids in static matrix. In this paper we report molecular dynamics simulation results for the static and dynamic properties of hard sphere fluids in matrices (or media) composed of quenched hard spheres.

There is a large body of work on the behavior of random walks in matrices composed of fixed obstacles. For a random walk in a Euclidean space, the mean-square displacement (MSD) is a linear function of time and the diffusion is referred to as normal or regular. In disordered systems, however, the diffusion can be anomalous, i.e., the MSD $\langle r^2 \rangle$ can vary sublinearly with time as $\langle r^2 \rangle \sim t^{2/d_w}$ with $d_w > 2$. The constant d_w is called the anomalous subdiffusion exponent, and normal diffusion is recovered for $d_w = 2$. Percolation theory has been used to describe diffusion in porous systems [1–3] modeled as a collection of static obstacles. In the absence of obstacles, the diffusion is normal. For a low concentration of the obstacles, the cluster of unobstructed sites (called a percolation cluster) is fractal over short distances and homogeneous at large distances. In this case, since the diffusion is self-similar at all length and time scales for a fractal system, the diffusion is anomalous at short distances and normal at larger distances. The characteristic distance (time) scale where the diffusion changes from anomalous subdiffusion to regular diffusion is called the crossover length (time). As the obstacle concentration increases, the crossover length increases, and at the percolation threshold concentration of the obstacles, the crossover length (time) diverges and the diffusion is anomalous over all distances (times).

There are many experimental studies of the diffusion of penetrants in disordered matrices, which support the qualitative picture described above. The long-time translational self-diffusion coefficient of spherical silica particles in porous glasses [4] and random sphere packings [5] with varying pore size and ionic strength [6] has been studied using dynamic light scattering and fluorescence recovery after photobleaching. The long-time tracer diffusion coefficient is found to be uniquely dependent on the ratio of the tracer size to the packing sphere size β, and vanishes when β is larger than ~ 0.15 for random close packing [5], since the tracer cannot escape from the interstitial holes. The anomalous subdiffusive regime becomes dominant as the percolation threshold is approached. Nuclear-magnetic-resonance microscopy studies of diffusion on quasi-two-dimensional random-site percolation clusters [7], close to the percolation threshold, suggest that normal diffusion limit is reached only at very long times. Anomalous subdiffusive behavior has also been observed for a variety of lipids and proteins in the plasma membrane of cells, using single-particle tracking measurements [8,9] and fluorescence photobleaching recovery [10,11]. Anomalous subdiffusion has a major effect on the mobility, and hence the kinetics of diffusion mediated

systems. Many factors such as obstruction, binding, hydrodynamic interactions, etc., are believed to contribute to the effects of membrane heterogeneities in lateral diffusion.

The long-time diffusion of solutes in disordered matrices can be studied using field theoretic formulations. For example, Chakraborty *et al.* [12] have presented a theory that describes the diffusion of ions in charged disordered matrices using a path integral representation for the propagator coupled with a field theory for the matrix. Using a variational method, they calculated the diffusion coefficient for the case of Gaussian spatial density fluctuations in the disorder. From numerical solution of their equations and asymptotic analysis they demonstrated a crossover from diffusive to subdiffusive behavior as the strength (i.e., density) of the disorder was increased, and suggested that the mechanism for ion motion change from diffusion to hopping for high strengths of the disorder [13]. This physical picture is consistent with other theories [14]. More recently, Witkoskie, Yang, and Cao [15] have investigated several approaches for Brownian motion in dynamically disordered matrices. They investigated the behavior of a diffusing particle using perturbation theory, and various treatments on the Martin-Siggia-Rose [16] functional.

Despite the practical and theoretical importance of these systems, there have been few computer simulation studies of the dynamics of fluids in quenched matrices, and little is known about the behavior of standard models. In fact, all the simulation studies we are aware of have focussed on a single solute in static matrices. Penetrant diffusion in glassy amorphous polymers has been studied using molecular dynamics [17,18] (MD) and Monte Carlo [19] (MC) simulations. The results indicate a hopping mechanism for the penetrants: the penetrants dwell in the voids of the polymer matrix for considerable time and perform fast jumps between neighboring voids. Normal diffusion is reached at long times, but over intermediate time scales an anomalous subdiffusive regime exists. Diffusion of ionic particles in charged disordered matrices indicates that the charge centers create deep traps that capture the mobile particles. However, at long times the mobile particles escape the traps and their motion between traps is diffusive [20]. MC simulations of diffusion in zeolites modeled as a network of well-defined sites also suggest a hopping mechanism for the diffusing molecules [21–24]. Diffusion in porous random matrices has been studied using Brownian dynamics simulations [25,26] and MC simulations in two [11,27–29] and three dimensions [30,31]. Although these simulation studies provide useful insight into the effect of disordered matrices on the fluid diffusion at infinitely dilute concentration, the study of a single tracer particle ignores the interaction between fluid particles themselves, which plays a significant role even in simple fluids.

In this paper we present molecular dynamics simulation results for the diffusion of hard spheres in a matrix of fixed hard spheres. The choice of model allows us to focus on excluded volume effects on the dynamics, and use a very efficient discontinuous molecular dynamics algorithm to evolve the system. We quantify the effect of matrix and fluid density, the ratio of the size of the fluid spheres to that of the matrix spheres, and the method of preparation of the matrix on the dynamics of the hard sphere fluid. Naive extension of existing theories for the diffusion of liquid mixtures is not in good agreement with simulations.

The rest of the paper is organized as follows. The molecular model and simulation methods are presented in Sec. II. The results are presented in Sec. III, and a summary and some conclusions are presented in Sec. IV.

II. SIMULATION DETAILS

The simulation cell is a cube with periodic boundary conditions in all directions. The fluid particles are modeled as hard spheres of diameter σ_{ff}, and the matrix is composed of fixed hard spheres of diameter σ_{mm}. Fluid spheres and matrix spheres also interact via a hard sphere potential, with diameter $\sigma_{fm}=(\sigma_{ff}+\sigma_{mm})/2$. The box length L is chosen to be large enough for fluid particles to show the normal diffusive behavior and contain enough fluid and matrix particles for good statistics: $L=11.026\sigma_{mm}$ in most cases and $13.892\sigma_{mm}$ for high densities of the quenched spheres. The number of matrix spheres, N_m, ranges from 128 to 1280 and the number of fluid spheres, N, ranges from 128 to 1024. The box length is adjusted to achieve the desired density. We also checked for finite size effects for some systems by performing simulations with simulation cells of different lengths and found no significant differences.

The simulation temperature T is defined by the equipartition theorem, which relates the temperature to the system kinetic energy by

$$\frac{3}{2}Nk_BT=\frac{1}{2}\sum_{i=1}^{N}m_iv_i^2, \tag{1}$$

where k_B is Boltzmann's constant and m_i is the mass of the fluid particles. The particle kinetic energy k_BT affects only the velocity distribution of fluid particles and is set to unity in this study. In addition, the matrix hard sphere diameter σ_{mm} and the mass m_f of fluid particles are the units of length and mass, respectively, and the unit of time is $\tau_{MD}\equiv\sqrt{m_f\sigma_{mm}^2/k_BT}$. These constants are set to unity in the results reported.

Starting with an initial configuration, the creation of which is discussed shortly, the system is evolved using the discontinuous molecular dynamics (DMD) simulation method [32–34]. In this method, the system is evolved via successive collisions. First, the time to the next collision is calculated and all the fluid atoms are translated forward until the collision occurs. Next, the postcollision velocities of the colliding pair are determined from the dynamics of an elastic collision. Finally, the properties of interest are calculated before returning to the first step. Since the time evolution is exact up to the machine precision, DMD is stable over long times. We use various optimization methods such as linked lists and neighbor lists. With these optimization algorithms, the computation time scales linearly with the number of particles in the system [33,34].

The simulation algorithm is similar to that of hard sphere fluids. The collision time t_{ij} between ith and jth particles is given by

$$|\mathbf{r}_{ij}(t+t_{ij})| = |\mathbf{r}_{ij} + \mathbf{v}_{ij}t_{ij}| = \sigma_{ij}, \tag{2}$$

where $\mathbf{r}_{ij}=\mathbf{r}_i-\mathbf{r}_j$, $\mathbf{v}_{ij}=\mathbf{v}_i-\mathbf{v}_j$, $\mathbf{r}_i$ is the position of sphere i, $\mathbf{v}_i$ is the velocity of sphere i, and σ_{ij} is the hard-sphere diameter between the two species. The resulting t_{ij} is

$$t_{ij} = \frac{-b_{ij} - \sqrt{b_{ij}^2 - v_{ij}^2(r_{ij}^2 - \sigma_{ij}^2)}}{v_{ij}^2}, \tag{3}$$

with $b_{ij}=\mathbf{r}_{ij}\cdot\mathbf{v}_{ij}$. Note that b_{ij} will be less than zero if the particles are going to collide. Post-collision velocities are determined from conservation of kinetic energy and linear momentum, i.e.,

$$\mathbf{v}_i^{new} = \mathbf{v}_i - \frac{2m_j}{m_i+m_j}(\hat{\mathbf{r}}_{ij}\cdot\mathbf{v}_{ij})\hat{\mathbf{r}}_{ij}, \tag{4}$$

$$\mathbf{v}_j^{new} = \mathbf{v}_j + \frac{2m_i}{m_i+m_j}(\hat{\mathbf{r}}_{ij}\cdot\mathbf{v}_{ij})\hat{\mathbf{r}}_{ij}, \tag{5}$$

where $\mathbf{v}_i^{new}$ is the postcollision velocity of sphere i, $\hat{\mathbf{r}}_{ij}=\mathbf{r}_{ij}/r_{ij}$ is the unit vector of $\mathbf{r}_{ij}$, and m_i is the mass of particle i. For collisions between fluid particles, where $m_i=m_j$,

$$\mathbf{v}_i^{new} = \mathbf{v}_i - \frac{b_{ij}}{\sigma_{ff}^2}\mathbf{r}_{ij}, \tag{6}$$

$$\mathbf{v}_j^{new} = \mathbf{v}_j + \frac{b_{ij}}{\sigma_{ff}^2}\mathbf{r}_{ij}. \tag{7}$$

For collisions between fluid particles and matrix particles, we assume that the mass of the matrix particle is infinite, and in this case,

$$\mathbf{v}_i^{new} = \mathbf{v}_i - \frac{2b_{ij}}{\sigma_{fm}^2}\mathbf{r}_{ij}. \tag{8}$$

The simulation starts with the generation of an initial configuration. Several methods for the generation of the random matrix are considered. In the major part of this study, the disordered matrix is generated by randomly inserting hard spheres into an empty simulation box and equilibrating this system using DMD. The resulting configuration is quenched (or fixed) and this serves as the disordered matrix for the incoming fluid molecules. The fluid molecules are then inserted into the matrix. A random location in the simulation cell is chosen, an attempt is made to insert a fluid sphere, and the insertion is accepted if there is no overlap between the sphere and other (fluid and matrix) spheres. This process fails at high volume fractions where most random insertions are unsuccessful. Therefore, at high volume fractions we employ the particle growth method [33,34], in which the fluid molecules are randomly inserted, but with a smaller diameter than desired. The diameter of each fluid sphere is grown randomly along with standard Monte Carlo translation moves until the desired particle size is achieved. The initial-configuration generation method used is similar to the particle insertion and deletion moves used in grand canonical Monte Carlo simulations, and might sample configuration space not accessible to usual diffusion experiments such as exclusion chromatography. There is therefore the possibility that the configuration might not be ergodic if, for example, a sphere is trapped in a region of matrix that is disconnected from other regions. We find that this occurs when the matrix volume fraction, $\phi_m[\equiv \pi N_m\sigma_{mm}^3/(6L^3)]$, is approximately greater than $\sim$0.20. This method of initial-configuration generation does mimic other experimental situations such as vesicle trafficking in living cells. The initial configurations are equilibrated using DMD until all fluid particles have moved roughly half the box length.

Properties are averaged over several trajectories for each realization of the disordered matrices, and then over several matrix configurations. Starting from the resulting equilibrated configurations, 1000 trajectories are stored at time intervals Δt_{sample}, chosen so that the fluid particles translate less than the distance L/N_s on average, where $N_s=256$ is the bin size. Static properties such as pair-distribution functions are calculated using the 1000 trajectories. Dynamic properties such as mean-square displacements are also obtained as a function of time, with a maximum time of $N_s\Delta t_{sample}$. The long-time self-diffusion coefficient D of fluid particles is calculated from the mean-square displacement $W(t)$ of each particle using the Einstein relation, i.e.,

$$D = \lim_{t\to\infty}\frac{W(t)}{6t} = \lim_{t\to\infty}\frac{\langle|\mathbf{r}_i(t+t_0)-\mathbf{r}_i(t_0)|^2\rangle}{6t}, \tag{9}$$

where $\mathbf{r}_i$ is the position of fluid particle i and t_0 is an arbitrary initial time. Only data points from $(N_s/2)\Delta t_{sample}$ to $N_s\Delta t_{sample}$ are used in calculating D. The static and dynamic properties obtained by the above procedure are only statistical averages of a particular realization of the disordered matrices. To obtain matrix-averaged properties, the same procedure is repeated for 8–32 different realizations of the matrices, depending on the matrix volume fraction. Error bars in this paper correspond to one standard deviation of the latter average.

III. RESULTS AND DISCUSSION

A. Effect of volume fraction of fluid and matrix

The long-time self-diffusion coefficient D of the fluid particles has a strong dependence on the concentration of the fluid and of the disordered matrix. Figure 1(a) depicts D as a function of the volume fraction ϕ_f of fluid particles [defined as $\phi_f\equiv\pi N\sigma_{ff}^3/(6L^3)$], for various volume fractions ϕ_m of the disordered matrix and for $\sigma_{ff}=\sigma_{mm}$. For all values of ϕ_m investigated, D decreases monotonically as ϕ_f is increased. For a given value of ϕ_m, the decrease of D with ϕ_f is roughly power law (linear on a logarithmic scale) for low ϕ_f and stronger than power law for high ϕ_f. For any value of ϕ_f the presence of disordered matrix slows down the translational motion of fluid molecules in a monotonic fashion. This is shown in Fig. 1(b), where the particle diffusion relative to that without the disordered matrix is plotted against ϕ_m (note that the ordinate is plotted on a logarithmic scale). $D(\phi_m=0)$ is the diffusion of the fluid at the same value of ϕ_f but

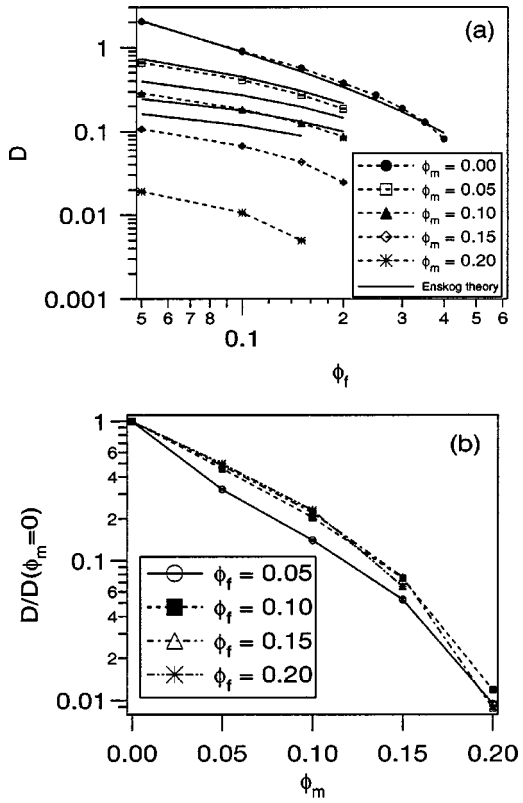

FIG. 1. (a) The long-time diffusion coefficient D of monoatomic fluid particles plotted as a function of the volume fraction of particles (ϕ_f) for different volume fractions of disordered matrix (ϕ_m). Results from the Enskog theory are also shown for comparison. (b) $D/D(\phi_m=0)$ plotted as a function of ϕ_m, where $D(\phi_m=0)$ is the diffusion coefficient of particles at the same value of ϕ_f, at $\phi_m=0$. Error bars from the simulations are smaller than the size of markers.

with $\phi_m=0$. The dependence of D on ϕ_m is similar for all values of ϕ_f, except at the lowest volume fraction $\phi_f=0.05$. The reason for the distinctive behavior for $\phi_f=0.05$ is mainly due to the strong concentration dependence of the fluid diffusion at low fluid volume fraction. For low fluid volume fractions, the diffusion constant is inversely proportional to its volume fraction (e.g., in Enskog theory which will be discussed below) but at higher fluid volume fractions, the dependence is much weaker. Therefore, the effect of the matrix volume fraction on the fluid diffusion is greater at low fluid volume fractions such as $\phi_f=0.05$ than at higher fluid volume fractions.

It is appealing to think of a fluid in a disordered matrix as a mixture of two components, where one of them is quenched in space. For the static properties, considerable progress has been made in the development of integral equations for these quenched annealed systems [35–50]. From a dynamical standpoint it is interesting to see if these systems can be mimicked by a binary mixture where one of the components is infinitely massive. To this end, we compare the simulation results to the Enskog theory for hard sphere mixtures at finite volume fractions [51]. Note that our fluid-matrix system does not satisfy the basic assumption of the theory since the fluid particles and the disordered matrix are not in thermal equilibrium. However, the theory might serve as a starting point for more sophisticated theories. According to the theory, the self-diffusion D_μ of species μ is given by

$$D_\mu = \frac{k_B T}{\xi_\mu^0(0)}, \tag{10}$$

with

$$\xi_\mu^0(0) = \frac{16\pi}{3}\left(\frac{k_B T}{2\pi}\right)^{1/2} \sum_\nu \left(\frac{m_\mu m_\nu}{m_\mu + m_\nu}\right)^{1/2} \rho_\nu \sigma_{\mu\nu}^2 g_{\mu\nu}(\sigma_{\mu\nu}), \tag{11}$$

where m_ν and ρ_ν are the mass and the number density, respectively, of species ν, $\sigma_{\mu\nu}$ is the hard sphere interaction diameter between species μ and ν, and $g_{\mu\nu}(\sigma_{\mu\nu})$ is the pair, distribution function at contact between species μ and ν. In the $m_m \to \infty$ limit, Eq. (11) takes the form

$$\xi_f^0(0) = 32\left(\frac{k_B T m_f}{2\pi\sigma_{ff}^2}\right)^{1/2}\left[\frac{1}{\sqrt{2}}\phi_f g_{ff}(\sigma_{ff}) + \left(\frac{\sigma_{fm}}{\sigma_{ff}}\right)^2 \phi_m g_{fm}(\sigma_{fm})\right]. \tag{12}$$

The theory requires the contact value of the pair correlation functions, which is obtained from the simulations.

The theoretical predictions for the self-diffusion coefficient of the fluid particles are plotted in Fig. 1(a). In the absence of the matrix, the theory is in quantitative agreement with simulations, as has been noted previously [34]. For low matrix volume fractions, i.e., $\phi_m=0.05$, the theory is still in reasonably good agreement with the simulation results, although it tends to overestimate D. The reason why the Enskog theory works well even in this regime is that the correlations between matrix particles are not very strong. As a consequence, the mobility of fluid particles is affected mainly by individual immobile obstacles rather than by their collective correlations, such as geometric constraints.

As the matrix volume fraction is increased further, however, the theory significantly overestimates the value of D, with an order of magnitude difference for $\phi_m=0.20$. This discrepancy between the Enskog theory and the simulation results at high matrix volume fractions is not surprising, because at high matrix volume fractions the configurations of the fluid and disordered matrix are very different from those of the equilibrium mixtures, which is the basic assumption in the Enskog theory.

The presence of many immobile obstacles hinders the dynamics of fluids not only due to the excluded volume interaction of each obstacle but also due to the geometric constraints induced by clusters of obstacles. This geometric effect is depicted in Fig. 2, which shows a snapshot of the disordered matrix disks (black solid circles) in two dimensions (2D), where the circle around a matrix disk represents the excluded area of each disk (assuming fluid particles have the same size as matrix) and the shaded area indicates an additional excluded area due to the geometric constraints caused by the surrounding matrix. Note that the excluded volume effect induced by geometric constraints is not present in fluid systems without static matrix. This additional ex-

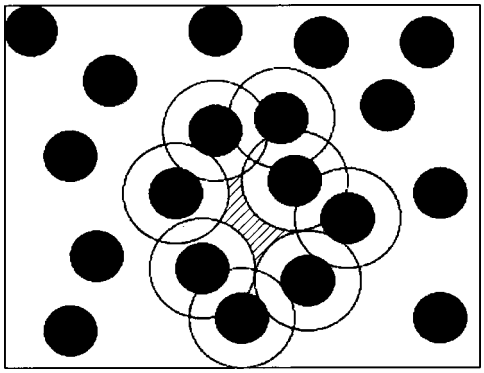

FIG. 2. A snapshot of disordered matrix disks (solid black circles) in 2D. The circle around each matrix disk represents the area excluded by each matrix (assuming fluid particles have the same size as matrix) and the shaded area indicates an additional excluded area due to the geometric constraint induced by the surrounding matrix disks.

cluded volume effect becomes significant at high matrix volume fractions, thus further slowing down the translation diffusion of the fluid particles.

The presence of static disordered matrix therefore has a greater effect on the translational motion of fluid particles than the presence of fluid particles themselves, i.e., at a fixed total volume fraction ($\phi_{tot}=\phi_f+\phi_m$), D decreases strongly as ϕ_m increases. For example, $D(\phi_f=0.05,\phi_m=0.20)$ is lower than $D(\phi_f=0.25,\phi_m=0)$ by an order of magnitude. This dynamic variation depending on the matrix and fluid volume fractions is not observed in the static correlations of the fluid and the disordered matrix. Figure 3 depicts the fluid-fluid (g_{ff}) and fluid-matrix (g_{fm}) pair correlations functions for various combinations of ϕ_f and ϕ_m, with $\phi_{tot}=0.25$. Although the first peak is slightly lower for higher values of ϕ_m, there is no significant difference in $g_{ff}(\sigma_{ff})$, which is the input for the Enskog theory. The fluid-matrix pair-distribution function g_{fm}, shown in Fig. 3(b), displays similar behavior except that the first peak becomes slightly higher as ϕ_m is increased. As a consequence, the Enskog theory or any theory based on just static correlations between species cannot describe the effect of static disordered matrix correctly.

In one and two dimensions the translational motion of a particle shows subdiffusive behavior on length scales smaller than the correlation length of the fractal, and recovers diffusive behavior at longer times [2]. At the so-called percolation threshold, the correlation length becomes infinite, and the motion of the particles is subdiffusive at all times. However, it is not clear whether this relation between subdiffusion and the percolation threshold is valid in three dimensions. In fact, we see no indication of subdiffusion at or over the percolation threshold, the volume fraction of which is ≈ 0.04 in three dimensions [36,52,53]. (In previous simulations [52], the percolation threshold for extended hard sphere systems, where two particles are assumed to be connected if their centers are within a distance d of each other, was reported to be $\rho_m d^3 \approx 0.65$ for $d=2\sigma_{mm}$. Therefore, the percolation threshold ϕ_m in volume fraction for our system is equal to $(\pi/6)\rho_m\sigma_{mm}^3=(\pi/48)\rho_m d^3=0.04$.) We do, however, observe that the crossover time when fluid particles begin to show

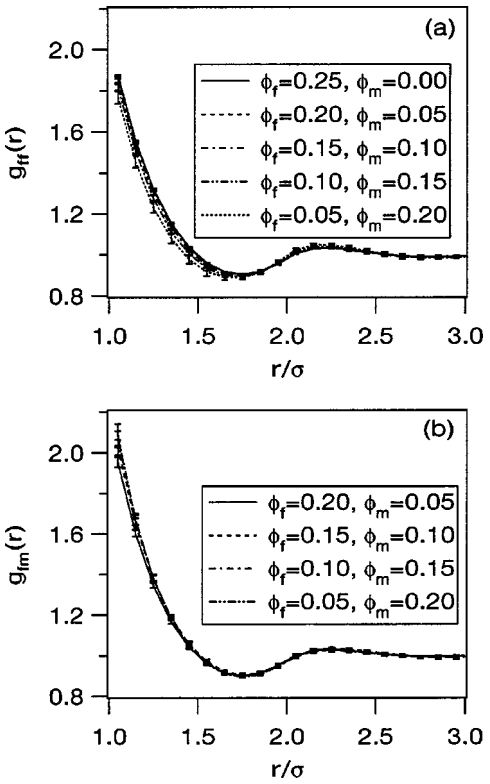

FIG. 3. (a) The fluid-fluid pair-distribution function g_{ff} shown for various combinations of the fluid (ϕ_f) and matrix (ϕ_m) volume fractions with the total volume fraction fixed at 0.25. (b) The fluid-matrix pair-distribution function g_{fm} shown for similar conditions as (a).

diffusive behavior from subdiffusive behavior becomes longer as the matrix volume fraction is increased. Figure 4(a) depicts the mean-square displacement $W(t)$ of fluid particles as a function of time t on a logarithmic scale for $\phi_f=0.05$ and various values of ϕ_m. Note that $W(t)$ is divided by 6 so that its slope on a logarithmic plot is equal to the corresponding diffusion coefficient in the diffusive limit. The slope of $\ln W(t)$ vs $\ln t$ is an indicator of diffusive or subdiffusive behavior, i.e., the slope is equal to one for diffusive behavior and is less than one for subdiffusive behavior. In most cases, we see diffusive behavior at long times. The exception is for $\phi_m=0.25$, when the slope fails to reach one within our simulation time. Inspection of trajectories of individual fluid particles indicates that some of the particles are trapped in a cage made by clusters of immobile matrix. To verify the effect of the trapping, we plot the probability distribution of $W(\tau)$ of fluid particles when τ is $2048\tau_{MD}$ for $\phi_m=0.20$ and $128\,000\tau_{MD}$ for $\phi_m=0.25$ in Fig. 4(b). Unlike the $\phi_m=0.20$ case, where the distribution is bell shaped and peaked near $\tau=100\tau_{MD}$, the distribution for $\phi_m=0.25$ shows a strong peak below $10\tau_{MD}$ and is almost flat for $\tau>30\tau_{MD}$. This strongly indicates that not only are a fraction of fluid particles at this high matrix fraction trapped in a local region but, in addition, even the diffusion of free fluid particles is highly heterogeneous.

There is no clear-cut distinction between trapped and free particles because the size distribution of traps created by the

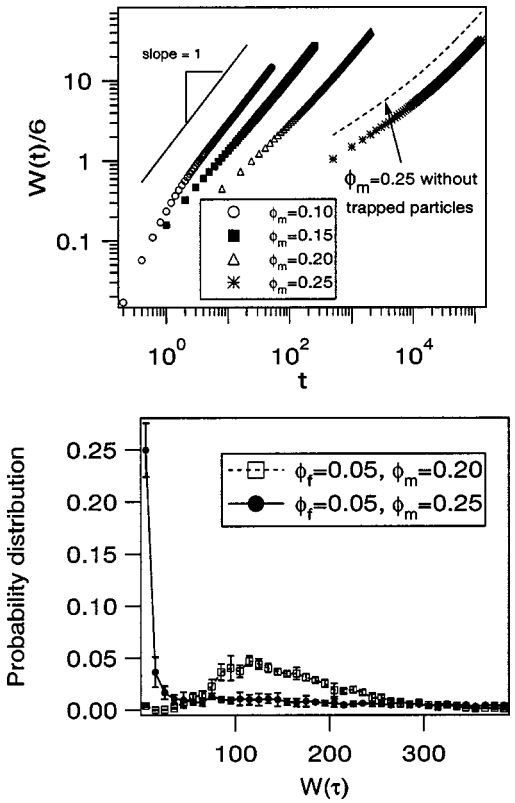

FIG. 4. (a) The mean-square displacement $W(t)$ of the fluid particles as a function of time at $\phi_f=0.05$ and various values of ϕ_m on a logarithmic scale. Note that $W(t)$ is divided by 6 so that the slope is equal to the corresponding diffusion coefficient in the diffusion limit. (b) The probability distribution of $W(\tau)$ at $\tau=2048\tau_{MD}$ for $\phi_m=0.20$ and $\tau=128\,000\tau_{MD}$ for $\phi_m=0.25$. The dashed line in (a) is the mean-square displacement of fluid particles, whose $W(\tau)$ is greater than $30\tau_{MD}$.

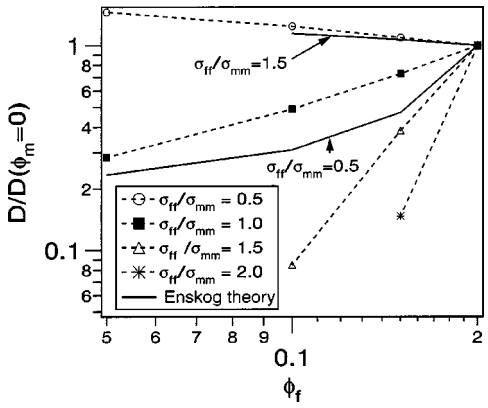

FIG. 5. The diffusion coefficient of spherical particles in the disordered matrix normalized by the diffusion coefficient of particles of the same size without matrix, $D/D(\phi_m=0)$, plotted as a function of the particle volume fraction ϕ_f for different values of the particle-particle exclusion diameter σ_{ff} at a fixed value of the particle-matrix exclusion, $\sigma_{mm}=1.0$. The total volume fraction, $\phi_{tot}=\phi_f+\phi_m$, is also fixed at 0.20 for all cases.

static matrix is expected to be polydisperse, which is manifested as the almost flat distribution of $W(t)$ for $\phi_m=0.25$. However, since it appears that the first three points in the distribution in Fig. 4(b) deviate from the other points, we exclude particle trajectories whose $W(\tau)$ is below $30\tau_{MD}$, and plot the mean-square displacement from the remaining particles as a dashed line in Fig. 4(a). Although the modified mean-square displacement is twice as large as the original one for the whole time range, its curvature remains the same, i.e., the subdiffusive behavior is persistent within the investigated simulation time scale even without trapped trajectories. The persistent subdiffusive behavior can be attributed to the heterogeneity of the particle diffusion as shown in Fig. 4(b). Because of this heterogeneous nature, the particle motion cannot be described using a single-diffusion coefficient.

B. Effect of particle size

The fluid dynamics are expected to be strongly dependent on the ratio of the diameters of fluid and matrix spheres. Figure 5 shows the diffusion coefficient of spherical particles in the disordered matrix normalized by the diffusion coefficient of particles of the same size in the absence of the matrix, $D/D(\phi_m=0)$, as a function of ϕ_f for different values of σ_{ff}, for a fixed value of $\sigma_{mm}=1.0$. The total volume fraction, $\phi_{tot}=\phi_f+\phi_m=0.20$ for all cases, and ϕ_m therefore decreases as ϕ_f increases. Interestingly, the diffusion coefficient shows a qualitatively different trend depending on the size ratio. When σ_{ff} is greater than or equal to σ_{mm}, $D/D(\phi_m=0)$ increases as ϕ_f increases. However, when $\sigma_{ff}=0.5$, the trend is reversed and the diffusion gets faster as ϕ_f decreases or more fluid particles turn into immobile matrix. Although it appears strange at first glance, this behavior can be explained qualitatively using the concept of free volume [54]. When σ_{ff} is greater than σ_{mm}, replacing a fluid particle with several fixed matrix of a smaller size increases the volume excluded to the particles and this slows down the translational motion of the fluid particles. On the other hand, when σ_{ff} is smaller than σ_{mm}, the diffusion of the fluid particles becomes faster when several small particles are replaced by a single immobile particle with a bigger size, thereby decreasing the volume excluded to the diffusing particles.

C. Effect of matrix structure

Initial configurations of the fluid particles and the immobile matrix are generated in simulations by initially equilibrating randomly generated matrix and then inserting fluid particles in the equilibrated matrix (method EQU). The matrix can be also generated in many other ways and it is of interest to examine the effect of matrix preparation on the dynamics of the particles. One way of generating initial configurations is via random sequential adsorption [41] (method RSA) of the disordered matrix, where the matrix is randomly generated (but not equilibrated as in method EQU), and the fluid particles are then inserted. Another way is to generate and equilibrate $N+N_m$ particles, and then randomly select N_m out of $N+N_m$ particles as the disordered matrix (method MIX). These three methods give different probability distributions for the disordered matrix. For example, the probabil-

ity distributions for method EQU and method MIX are, respectively, given by

$$P_{EQU}(\mathbf{r}_1, \ldots, \mathbf{r}_{N_m}) = \frac{\exp\left[-\beta U(\mathbf{r}_1, \ldots, \mathbf{r}_{N_m})\right]}{Z_{N_m}} \tag{13}$$

and

$$P_{MIX}(\mathbf{r}_1, \ldots, \mathbf{r}_{N_m}) = \frac{\int \cdots \int \exp\left[-\beta U(\mathbf{r}_1, \ldots, \mathbf{r}_{N_m}, \mathbf{r}_{N_m+1}, \ldots, \mathbf{r}_{N_m+N})\right] d\mathbf{r}_{N_m+1} \cdots d\mathbf{r}_{N_m+N}}{Z_{N_m+N}}, \tag{14}$$

where $U(\mathbf{r}_1, \ldots, \mathbf{r}_{N_m+N})$ is the potential energy of a configuration of N_m+N particles, and Z_{N_m+N} is the configuration integral. The probability distribution for method RSA is also different from the above two [41].

This difference in the matrix structure has only a slight effect on the pair correlation function of the fluid but a significant effect on the dynamic properties. The particle-particle pair correlation function $g_{ff}(r)$ of spherical fluid particles at $\phi_f=0.10$ and $\phi_m=0.20$ is shown for the three methods in Fig. 6(a). Note that $g_{ff}(r)$ of method MIX exactly matches the pair correlation function of particles at $\phi_f=0.30$ without matrix. There is a noticeable discrepancy between the different methods at short distances, but overall the three methods have similar results for the pair correlation functions. The matrix structure has a greater effect on the dynamics of particles. Figure 6(b) depicts the diffusion coefficient of fluid particles in the three different matrix structures as a function of ϕ_f, for two values of ϕ_m. At $\phi_m=0.1$, there is little difference among three methods, although D of method MIX is slightly higher than the other two methods. However, at a higher value of ϕ_m, D is clearly different by as much as an order of magnitude, for the three different matrix structures. The fact that the disordered matrix is not fully characterized by its volume fraction was also pointed out by Arns *et al.* [55].

D. Analysis of trajectories with the single-chain structure factor

The trajectory of each particle maps out a path in space and this path may be visualized as the conformation of a single-polymer molecule. The average shape of these trajectories can then be analyzed using the methods of polymer statistics. Since a particle at any given time does not interact with itself (or another particle) at another time, these trajectories are analogous to an ensemble of noninteracting "ideal" polymers in a sea of obstacles, with the position of the particle at a time $t_i=i\Delta t$ corresponding to the position of the ith monomer in the polymer chain. We analyze particle trajectories using this analogy, by setting the degree of polymerization (or the number of particle positions in a trajectory) to 256, and varying the time step Δt to study the fluid behavior on various time scales. The average shape of the polymer chain contains information regarding the dynamics of the particles.

Single-chain conformational properties are often analyzed in terms of the single-chain structure factor $\omega(k)$ defined by

$$\omega(k) = \frac{1}{N_m} \sum_{i,j}^{N_m} \left\langle \frac{\sin(kr_{ij})}{kr_{ij}} \right\rangle, \tag{15}$$

where k is the reciprocal wave vector, N_m is the degree of polymerization, r_{ij} is the distance between the ith and jth monomers in a single chain, and $\langle A \rangle$ is the ensemble average over all chain conformations. The single-chain structure factor displays characteristic behavior on various length scales.

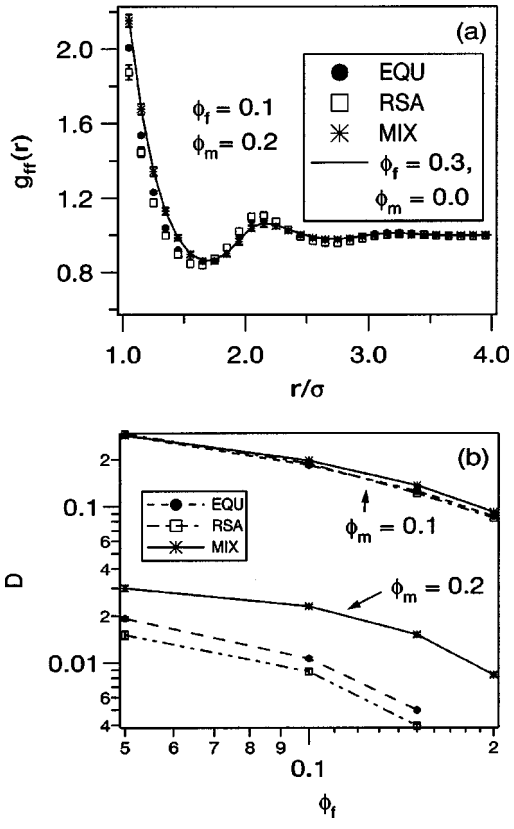

FIG. 6. (a) The particle-particle pair correlation function $g_{ff}(r)$ at $\phi_f=0.1$ and $\phi_m=0.2$ for three different matrix structures. The solid line also shows $g_{ff}(r)$ at $\phi_f=0.3$ without matrix for comparison. (b) The diffusion coefficient D plotted as a function of ϕ_f for $\phi_m=0.1$ and 0.2.

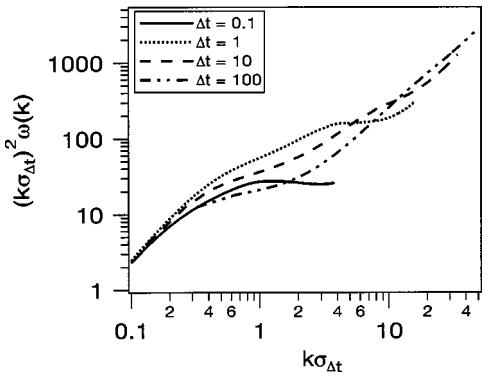

FIG. 7. Single-chain structure factor $\omega(k)$ multiplied by $(k\sigma_{\Delta t})^2$ is plotted as a function of wave vector $k\sigma_{\Delta t}$ at $(\phi_f, \phi_m) = (0.10, 0.20)$. The average displacement $\sigma_{\Delta t}$ is $0.148\sigma_{ff}$, $0.613\sigma_{ff}$, $1.34\sigma_{ff}$, and $3.19\sigma_{ff}$ for $\Delta t = 0.1$, 1, 10, and 100, respectively.

For low wave vectors ($kR_g \ll 1$, where R_g is the radius of gyration of the polymer) $k^2\hat{\omega}(k) \sim N_m k^2(1 - k^2R_g^2/3 + \cdots)$ and for high wave vectors $\hat{\omega}(k) \sim 1$. In the intermediate scaling regime, the single-chain structure factor provides information regarding the shape of the chain. Consider a sphere of radius r around a central bead so that m beads are present inside the sphere. If $r^2 \sim m^{2\nu}$ then $\omega(r) \sim m/r^3$ implies $\omega(r) \sim r^{1/\nu - 3}$. Taking the Fourier transform and using the scaling trick, one obtains $\hat{\omega}(k) \sim k^{-1/\nu}$ over the range of length scales of the order of the size of the chain. For an ideal chain, $\nu = 1/2$, and $k^2\hat{\omega}(k) \sim 1$ in the scaling regime. It is therefore customary to plot $k^2\hat{\omega}(k)$ versus k on what is called a Kratky plot.

An important difference between a diffusing particle and a polymer chain is that in the former case the location of each monomer is arbitrary, while in the latter it arises from chemical interactions. The unit of wave vector k for a given time step is $(\sigma_{\Delta t})^{-1}$, where $\sigma_{\Delta t}$ is the average displacement of each fluid particle during interval Δt. The value of $\sigma_{\Delta t}$ was $0.148\sigma_{ff}$, $0.613\sigma_{ff}$, $1.34\sigma_{ff}$, and $3.19\sigma_{ff}$ for $\Delta t = 0.1$, 1, 10, and 100, respectively. We use a reduced variable $k\sigma_{\Delta t}$ instead of k in analyzing the trajectories. We average over all trajectories of all particles for a given state point.

Fluid particles without disordered matrix show diffusive behavior at all time scales except at very short-time scales, when the ballistic motion is observed. A Kratky plot therefore shows linearly increasing behavior for short Δt and a plateau behavior for large enough Δt. $\omega(k)$ in a disordered matrix is very different from that in neat fluids, with qualitatively different behavior on different time scales. Figure 7 depicts $(k\sigma_{\Delta t})^2\omega(k)$ as a function of $k\sigma_{\Delta t}$ for four different values of Δt, and for $\phi_f = 0.1$ and $\phi_m = 0.2$. For $\Delta t = 0.1$, $(k\sigma_{\Delta t})^2\omega(k)$ shows a negative slope in the range of $k\sigma_{\Delta t} = 1 - 4$, which suggests that particle motion in the presence of immobile disordered matrix is localized at a local region at this short-time scale, i.e., the polymer chain is collapsed ($\nu < 0.5$). As the time step is increased to $\Delta t = 1$, the negative slope disappears but a plateau region is seen around $k\sigma_{\Delta t} = 4 - 10$ in $(k\sigma_{\Delta t})^2\omega(k)$, indicating that particles diffuse normally on this time scale. Interestingly, when the time step is further increased ($\Delta t = 10$), the particle motion deviates from the normal diffusion, showing a monotonic increase in $(k\sigma_{\Delta t})^2\omega(k)$ with $k\sigma_{\Delta t}$. This superdiffusive behavior might be the signature of the particle hopping process, where particles hop from one vacant site to another occasionally while they stay at local sites most of the time. Although the process gives the same mean-square displacement as normal diffusion [56], the trajectories are different, i.e., they are extended on intermediate time scales, but after sufficiently many hops, they become diffusive. This normal diffusion at long times is also seen in our study (see the plateau regime around $k\sigma_{\Delta t} = 1$ in Fig. 7 at $\Delta t = 100$).

IV. SUMMARY AND CONCLUSIONS

We report results of discontinuous molecular dynamics simulations of hard sphere fluids in disordered matrices composed of hard spheres. The effect of fluid and matrix densities, matrix structure, and particle size on the mean-square displacement, long-time self-diffusion, and single-chain structure factor of particle trajectories are presented and analyzed.

The matrix volume fraction has a stronger effect on fluid diffusion than the fluid itself, especially at high matrix volume factions. We attribute this to the geometric constraints produced by disordered matrix which results in strong hindrance of fluid diffusion. Replacing fluid particles with an equal number of matrix particles with the same size decreases the diffusion of fluids. This trend can be reversed if the matrix particles are larger than that of fluid particles, however, even when the total volume fraction is fixed. The way the matrix structure is prepared has also great impact on the fluid diffusion, especially at high matrix volume fractions. Although the static correlations between fluid and matrix particles are similar for the different preparation methods, the diffusion coefficient can be different by an order of magnitude. Therefore, the dynamic behavior of fluids cannot be described using only static information. Simple extensions of theories for mixtures to this system by setting the mass of the matrix spheres to infinity therefore fail. We also anticipate that mode-coupling theories, which rely only on static input regarding the system, will also fail.

The single-chain structure factor $\omega(k)$, which is popularly used in polymer community, can be used to analyze the fluid behavior at different time scales. Unlike neat fluids (fluids without disordered matrix), fluids in disordered matrix show different behavior of $\omega(k)$, depending on the time scale studied. At very short-time scales, there is a negative slope in $k^2\omega(k)$ suggesting the trajectories are localized. On longer time scales, particle trajectories are more extended than a random walk and normal diffusion is recovered on very long-time scales. This change in particle diffusive behavior might be the signature of the hopping process.

We conclude that the dynamics of simple hard sphere liquids in quenched random matrix is very interesting. The effect of fluid-fluid and fluid-matrix interactions, and the struc-

ture and dynamics of the matrix itself are natural extensions of this work. In addition the rotational dynamics of molecular liquids could shed considerable light into the dynamics of liquids in glassy materials, and possible to carry out with simple extensions of our algorithm. Work along these lines is currently in progress.

ACKNOWLEDGMENTS

We gratefully acknowledge support from the National Science Foundation (through Grant No. CHE 0315219 to A.Y. and Grant No. CHE 0091916 to the Department of Chemistry).

[1] D. Stauffer and A. Aharony, *Introduction to Percolation Theory*, 2nd ed. (Taylor and Francis, London, 1992).
[2] S. Havlin and D. Den-Avraham, Adv. Phys. **36**, 695 (1987).
[3] A. Bunde and S. Havlin, *Fractals and Disordered Systems* (Springer, Berlin, 1991).
[4] S. G. J. M. Kluijtmans, J. K. G. Dhont, and A. P. Philipse, Langmuir **13**, 4982 (1997).
[5] S. G. J. M. Kluijtmans and A. P. Philipse, Langmuir **15**, 1896 (1999).
[6] S. G. J. M. Kluijtmans, E. H. A. de Hoog, and A. P. Philipse, J. Chem. Phys. **15**, 1896 (1998).
[7] A. Klemm, R. Metzler, and R. Kimmich, Phys. Rev. E **65**, 021112 (2002).
[8] R. N. Ghosh and W. W. Webb, Biophys. J. **66**, 1301 (1994).
[9] P. R. Smith, I. E. G. Morrison, K. M. Wilson, N. Fernandez, and R. J. Cherry, Biophys. J. **76**, 3331 (1999).
[10] T. J. Feder, I. Brust-Mascher, J. P. Slattery, B. Baird, and W. W. Webb, Biophys. J. **70**, 2767 (1996).
[11] M. J. Saxton, Biophys. J. **81**, 2226 (2001).
[12] A. K. Chakraborty, D. Bratko, and D. Chandler, J. Chem. Phys. **100**, 1528 (1994).
[13] Y. C. Zhang, Phys. Rev. Lett. **56**, 2113 (1986).
[14] M. W. Deem and D. Chandler, J. Stat. Phys. **76**, 911 (1994).
[15] J. B. Witkoskie, S. Yang, and J. Cao, Phys. Rev. E **66**, 051111 (2002).
[16] P. C. Martin, E. D. Siggia, and H. A. Rose, Phys. Rev. A **8**, 423 (1973).
[17] H. Takeuchi, J. Chem. Phys. **93**, 2062 (1990).
[18] F. M. Plathe, J. Chem. Phys. **94**, 3192 (1990).
[19] M. L. Greenfield and D. N. Theodorou, Macromolecules **34**, 8541 (2001).
[20] A. R. Mehrabi and M. Sahimi, Phys. Rev. Lett. **82**, 735 (1998).
[21] M. O. Coppens, A. T. Bell, and A. K. Chakraborty, Chem. Eng. Sci. **53**, 2053 (1998).
[22] L. G. Chen, M. Falcioni, and M. W. Deem, J. Phys. Chem. B **104**, 6033 (2000).
[23] A. I. Skoulidas and D. S. Scholl, J. Phys. Chem. B **105**, 3151 (2001).
[24] A. I. Skoulidas and D. S. Scholl, J. Phys. Chem. B **106**, 5058 (2002).
[25] I. C. Kim and S. Torquato, J. Chem. Phys. **96**, 96 (1991).
[26] L. Johansson and J.-E. Löfroth, J. Chem. Phys. **98**, 7471 (1993).
[27] M. J. Saxton, Biophys. J. **66**, 394 (1994).
[28] V. Pham and M. W. Deem, J. Phys. A **31**, 7235 (1998).
[29] M. Saadatfar and M. Sahimi, Phys. Rev. E **65**, 036116 (2002).
[30] P. A. Netz and T. Dorfmüller, J. Chem. Phys. **103**, 9074 (1995).
[31] N. C. Karayiannis, V. G. Mavrantzas, and D. N. Karayiannis, Chem. Eng. Sci. **56**, 2789 (2001).
[32] M. P. Allen and D. J. Tildesley, *Computer Simulation of Liquids* (Oxford University Press, New York, 1987).
[33] S. W. Smith, C. K. Hall, and B. D. Freeman, J. Chem. Phys. **102**, 1057 (1995).
[34] S. W. Smith, C. K. Hall, and B. D. Freeman, J. Comput. Phys. **134**, 16 (1997).
[35] Y. C. Chiew, G. Stell, and E. D. Glandt, J. Chem. Phys. **83**, 761 (1985).
[36] T. DeSimone, S. Demoulini, and R. M. Stratt, J. Chem. Phys. **85**, 391 (1986).
[37] W. G. Madden and E. D. Glandt, J. Stat. Phys. **51**, 537 (1988).
[38] Y. Chiew and G. Stell, J. Chem. Phys. **90**, 4956 (1989).
[39] L. A. Fanti, E. D. Glandt, and W. G. Madden, J. Chem. Phys. **93**, 5945 (1990).
[40] D. Chandler, J. Phys.: Condens. Matter **3**, F1 (1991).
[41] J. A. Given, J. Chem. Phys. **45**, 816 (1992).
[42] J. A. Given and G. Stell, J. Chem. Phys. **97**, 4573 (1992).
[43] W. G. Madden, J. Chem. Phys. **96**, 5422 (1992).
[44] E. Lomba, J. A. Given, and G. Stell, Phys. Rev. E **48**, 233 (1993).
[45] M. L. Rosinberg, G. Tarjus, and G. Stell, J. Chem. Phys. **100**, 5172 (1994).
[46] J. A. Given and G. Stell, Physica A **209**, 495 (1994).
[47] J. A. Given, J. Chem. Phys. **102**, 2934 (1995).
[48] E. Kierlik, M. L. Rosinberg, G. Tarjus, and P. A. Monson, J. Chem. Phys. **106**, 264 (1997).
[49] Y. C. Chiew, J. Chem. Phys. **110**, 10 482 (1999).
[50] A. Yethiraj, J. Chem. Phys. **116**, 5910 (2002).
[51] D. A. McQuarrie, *Statistical Mechanics* (Harper and Row, New York, 1976).
[52] A. L. R. Bug, S. A. Safran, G. S. Grest, and I. Webman, Phys. Rev. Lett. **55**, 1896 (1985).
[53] T. DeSimone, R. M. Stratt, and S. Demoulini, Phys. Rev. Lett. **56**, 1140 (1986).
[54] A. P. Minton, J. Biol. Chem. **276**, 10 577 (2001).
[55] C. H. Arns, M. A. Knackstedt, and K. R. Mecke, Phys. Rev. Lett. **91**, 215506 (2003).
[56] D. Nykypanchuk, H. H. Strey, and D. A. Hoagland, Science **297**, 987 (2002).